Assessing the potential of using chaotic advection flow for thermal food processing in heating tubes

Tian, Shuai; Barigou, Mostafa

DOI:
10.1016/j.jfoodeng.2015.12.005

Document Version
Peer reviewed version

Citation for published version (Harvard):
Tian, S & Barigou, M 2016, 'Assessing the potential of using chaotic advection flow for thermal food processing in heating tubes', *Journal of Food Engineering*, vol. 177, pp. 9-20. https://doi.org/10.1016/j.jfoodeng.2015.12.005

Accepted Manuscript

Assessing the potential of using chaotic advection flow for thermal food processing in heating tubes

Shuai Tian, Mostafa Barigou

PII: S0260-8774(15)30076-5

DOI: 10.1016/j.jfoodeng.2015.12.005

Reference: JFOE 8419

To appear in: *Journal of Food Engineering*

Received Date: 27 March 2015

Revised Date: 6 November 2015

Accepted Date: 13 December 2015

Please cite this article as: Tian, S., Barigou, M., Assessing the potential of using chaotic advection flow for thermal food processing in heating tubes, *Journal of Food Engineering* (2016), doi: 10.1016/j.jfoodeng.2015.12.005.

ASSESSING THE POTENTIAL OF USING CHAOTIC ADVECTION FLOW FOR THERMAL FOOD PROCESSING IN HEATING TUBES

Shuai Tian and Mostafa Barigou*

School of Chemical Engineering, University of Birmingham, Edgbaston, Birmingham, B15 2TT, UK

Abstract

Most food materials tend to be viscous and in general flow in the laminar regime. In continuous food sterilisation, the non-uniform velocity profile which characterises viscous flow coupled with a non-uniform temperature distribution result in a wide variation of product sterility and nutritional quality across the tube. The challenge is to be able to sterilise the fastest parts in the core region of the tube without over-processing too much the slowest parts near the wall. Chaotic advection is an alternative to turbulence, and uses the stretching and folding property of chaotic flows to promote fluid mixing at low Reynolds numbers. The use of inline static mixers or vortex generators to promote radial mixing and, thus, heat transfer and temperature uniformity, generates large pressure drops but more importantly these devices are unhygienic. We use a validated Computational Fluid Dynamics (CFD) model to show that mechanical vibration is an effective source of chaotic advection. The superimposition of a transverse harmonic motion on the flow of a single-phase viscous fluid in a heating tube, leads to large improvements in thermal processing uniformity and efficiency compared with a conventional process with or without an inline static mixer fitted. Results show that high levels of sterility, processing uniformity and product quality can be achieved in relatively short heating tubes, thus, potentially obviating the need for a holding stage.

Keywords: CFD, chaotic advection, continuous sterilisation, food quality, food sterility, vibration, viscous flow

1. Introduction

Radial heat transfer in laminar tube flow is governed by slow conduction which leads to a wide radial temperature distribution that poses a considerable challenge in many manufacturing processes. In continuous food sterilisation the non-uniform velocity profile which characterises viscous flow coupled with a non-uniform temperature distribution means that the coldest parts of the fluid at the centre of the tube travel the fastest, thus, resulting in a wide variation of product sterility and nutritional quality across the tube. The challenge is to be able to sterilise the fastest parts in the core region of the tube without over-processing too much the slowest parts near the wall. Increasing the temperature of the inner regions of the fluid is highly desirable so that ideally all parts of the fluid receive equal thermal treatment. Furthermore, better uniformity in the temperature profile helps reduce local variations in the fluid rheological properties which cause distortions in the velocity profile, thus making the flow behaviour of the fluid more predictable. To improve the uniformity of the temperature distribution, methods of increasing radial mixing are required. This problem has been recognised for a long time but effective technological solutions are still missing (Jung and Fryer, 1999).

Radial mixing can be achieved by turbulent flow conditions but the usually high fluid viscosities encountered in practice often make this proposition impractical and/or uneconomical. Alternatively, the use of inline static mixers (Hobbs and Muzzio, 1997; Saatdjian et al., 2012) or vortex generators (Chagny et al., 2000) is prohibited in hygienic processes because of the risk of contamination for their complex geometries promote fouling and make them difficult to clean. A considerable number of studies have demonstrated the effects of pulsating flow or mechanical oscillation on the heat flux and Nusselt number in tube flows (Klaczak, 1997; Gundogdu and Carpinlioglu, 1999; Lee and Chang, 2003). However, the effects on the radial temperature distribution and the development of the thermal boundary layer in a tube have not been reported.

Research has shown that mixing in non-turbulent flows can be greatly enhanced by complicated particle behaviour caused by chaotic advection. Chaotic advection is a concept derived from nonlinear dynamics and is widely used as an approach to investigate transport and mixing problems in fluid flows (Aref, 1984; 1990; Ottino, 1989). In applications where one wants to maximise the rate of mixing of flows, advection is used to accelerate the molecular diffusion process. The classical way to achieve this is through turbulence by using high Reynolds numbers to instigate the formation of a Kolmogorov energy cascade from large to small eddy scales, which results in small-scale structures that lead to rapid molecular diffusion and flow homogenisation. Chaotic advection affords a different mechanism to generate small-scale structures by exploiting the stretching and folding property of chaotic flows whose Lagrangian dynamics quickly evolves into a complex flow pattern. Mixing by chaotic advection is a purely kinematic process which does not require high Reynolds numbers. It has the advantages over turbulence that it does not require the high energy inputs needed to maintain the Kolmogorov cascade in turbulent mixing and can, thus, be exploited in situations where high Reynolds numbers cannot be used. Mechanical vibration is an effective mechanism by which such chaotic advection can be introduced in viscous flow (Eesa and Barigou, 2011; Tian and Barigou, 2015). In this study, we use a validated Computational Fluid Dynamics (CFD) model to demonstrate the large positive effects that a superimposed transverse harmonic motion can have on the extent and uniformity of heat treatment in single-phase laminar tube flow, and the potential benefits it can have for continuous in-flow sterilisation of viscous food fluids.

2. Theory

2.1 Temperature-dependent fluid viscosity model

The single-phase fluid used is an incompressible, temperature-dependent Newtonian fluid whose viscosity is assumed constant at a given temperature and is described by the well-known Arrhenius relationship:

$$\mu = k_0 exp\left(\frac{E_a}{R_g T}\right) \quad (1)$$

where k_0 is a pre-exponential factor, R_g is the ideal gas constant, T is temperature and E_a is the activation energy for viscosity. The constants k_0 and E_a are determined experimentally and their values for various fluids have been reported in the literature (e.g. Steffe, 1996). These parameters, as well as other physical properties (density ρ, specific heat capacity C_p, and thermal conductivity λ) were assumed constant and their values are given in Table1.

2.2 Transverse harmonic motion

In its basic form (**VF**), the technique uses transverse mechanical oscillations imposed on the tube wall in a direction perpendicular to the tube axis, as illustrated in Figure 1(*a*), and the wall displacement x is described by the harmonic function:

$$x = A\sin(\omega t) \quad (2)$$

where A is the amplitude of vibration, t is time, and ω is the angular function of the frequency of vibration, f, such that $\omega = 2\pi f$. The linear transversal velocity of the tube wall is then:

$$u = \frac{dx}{dt} = A\omega\cos(\omega t) \quad (3)$$

In the new enhanced form of the technique (**VF-SR**), the tube is continuously oscillated transversally but the orientation of oscillation is rotated instantly in a stepwise manner by an angle of 45 degrees about the tube axis, as depicted in Figure 1(*b*). The time interval, Δt, between change of orientation steps, needs to be optimized for a given set of process conditions. For the conditions considered in this work, a value $\Delta t \sim 10$ s was determined by numerical experimentation, thus, the frequency of the step rotation, Ω, is (and is expected to always be) very low compared with the frequency of lateral oscillations; for example, in this case $\Omega = 0.1$ Hz compared to $f = 50$ Hz. The effects of Ω on the thermal process are further discussed below.

Under steady state, the flow regime was always laminar with a Reynolds number $(Re = \rho\overline{w}D/\mu)$ within the range 1.4 – 90, where D is tube diameter and $\overline{w}$ is mean axial velocity. When the tube was vibrated, the vibration Reynolds number $\left(Re_v = \frac{\rho A\omega D}{\mu}\right)$ was within the range 22 – 1400; so flow remained laminar under all conditions of flow and temperature.

2.3 Governing equations

The governing transport equations which are the basis of the CFD model can be written in their general form (Bird et al., 1987), thus:

Continuity: $$\nabla \cdot \boldsymbol{U} = 0 \quad (4)$$

Momentum: $$\rho \frac{\mathrm{D}\boldsymbol{U}}{\mathrm{D}t} = -\nabla p + \nabla^2 \mu \boldsymbol{U} + \rho \boldsymbol{g} \quad (5)$$

Energy: $$\rho C_p \frac{\mathrm{D}T}{\mathrm{D}t} = \lambda \nabla^2 T + \mu \dot{\gamma}^2 \quad (6)$$

where p is fluid pressure, $\boldsymbol{g}$ is gravitational acceleration, $\boldsymbol{U}$ is the velocity field and $\dot{\gamma}$ is the second invariant of the shear rate tensor, defined as $\dot{\gamma} \equiv \left[\frac{1}{2}(\dot{\gamma}:\dot{\gamma})\right]^{\frac{1}{2}}$.

2.4 In-flow sterility and quality

Food sterility and quality levels can be calculated using the standard Eqs. (7) and (8), respectively:

$$F = \int_0^t 10^{(T-T_{Fref})/z_F}\, dt \quad (7)$$

where, F which is known as the F-value, is an equivalent heating time for which the product could be held at a constant reference temperature, T_{Fref}, to give the same final concentration of microbial pathogens as a processing time, t, for which the temperature, T, changes. T_{Fref} depends on the organism being inactivated or the indicator organism used in the process, e.g. 121.1 °C for the pathogen *C. botulinum*, and z_F is the temperature change which produces a 10-fold change in reaction rate from the rate at the reference temperature, e.g. z_F = 10 °C for *C. botulinum* (Jung and Fryer, 1999).

Product quality loss is estimated using the cook value, C, also known as the C-value, a parameter defined in a similar way to the F-value, which gives a measure of the extent of nutrient loss in units of time:

$$C = \int_0^t 10^{(T-T_{Cref})/z_C}\, dt \quad (8)$$

where T_{Cref} is a reference temperature dependant on the nutrient under consideration, e.g. 121.1 °C, and z_C is the temperature change which produces a 10-fold change in reaction rate from the rate at the reference temperature, e.g. z_C = 48 °C for thiamine destruction (Jung and Fryer, 1999).

It should be noted that Eq. (7) for the F-value, was originally derived for a static batch system and applies to materials where all the food has the same temperature-time profile (Ball and Olson, 1957; Jung and Fryer, 1999; Hui, 2006). In a continuous flow such as the one considered here, different fluid elements have different thermal histories and are subjected to different levels of microbial lethality. Therefore, as described below in Section (3.2), Eq. (7) is integrated along a given fluid trajectory whose thermal history is described by a computed $T(t)$ profile to give the local value of in-flow sterility at any given point in the flow within the computational grid. The same calculation process applies to in-flow quality C.

2.5 Uniformity of radial distribution of in-flow sterility and quality

The coefficient of variation, C_v, is used as a measure of sterility and quality uniformity across the tube and is usually defined as the ratio of the standard deviation, σ, to the volume-flowrate weighted mean value, $\overline{F}$ or $\overline{C}$. However, it should be noted that when the mean value is small, such a definition can lead to artificially high values of C_v. To avoid such erroneous values, we use a modified coefficient of variation, such that for F:

$$C_{v\text{-}F} = \frac{\sigma_F}{\overline{F}-\overline{F}_{ideal}} \tag{9}$$

where $\overline{F}_{ideal}$ is the volume-flowrate weighted mean value achieved at a given axial position z of an ideal plug flow having the same inlet conditions of mean velocity and temperature as the actual laminar flow.

The volume-flowrate weighted mean sterility across the tube, $\overline{F}$, is obtained by dividing the tube cross-section into a large number of cells (N = 1860), as shown in Figure 2, which can be identified by their polar coordinates r and θ. The analysis was conducted using this regular grid implemented in MATLAB to avoid the difficulties associated with the complex and varied cell shapes of the computational CFD grid. The sterility and axial velocity in a given cell are denoted by $F(r,\theta)$ and $w(r,\theta)$, respectively, and are considered at their nearly constant time-average values reached after a vibration time equivalent to the fluid residence time in the tube. Thus, $\sum_{i=1}^{N} w(r,\theta)S(r,\theta) = Q$ represents the volumetric flowrate through a cell, where $S(r,\theta)$ is the cross-sectional area of the cell. The volume-flowrate weighted mean sterility is, therefore, given by:

$$\overline{F} = \frac{1}{Q}\sum_{i=1}^{N} F(r,\theta)w(r,\theta)S(r,\theta) \tag{10}$$

In the limit as $S(r,\theta) \to 0$, i.e. for large N, the uniformity of the sterility distribution over the tube cross-section can be well described by the standard deviation:

$$\sigma_F = \sqrt{\frac{1}{Q^2}\sum_{i=1}^{N}\left[F(r,\theta)w(r,\theta)S(r,\theta) - \overline{F}w(r,\theta)S(r,\theta)\right]^2} \tag{11}$$

and the coefficient of variation $C_{v\text{-}F}$ (Eq. 9).

Similarly, the above relationships can be used to evaluate the standard deviation, σ_C, and coefficient of variation, $C_{v\text{-}C}$, for the quality, C.

3. CFD model

3.1 Simulations

3.1.1 Geometries and meshing

Three-dimensional simulations were set up and executed using the commercial software package ANSYS Workbench 14.5. The flow geometries were created and meshed using the software ICEM, while flow specification, solving and post-processing were all performed using CFX 14.5. In its basic form, the geometry consisted of a straight tube 30 mm in diameter and 2400 mm in length with three surface boundaries: inlet,

outlet, and wall (Figure 1(*c*)). The geometry was meshed with hexahedral cells. To optimise the mesh size it was necessary to carry out a mesh-independence study; this was done by performing a number of simulations with different mesh sizes, starting from a coarse mesh and refining it until results were no longer dependent on the mesh size. The mesh thus achieved contained approximately 4000 hexahedral cells per centimetre of tube length and around 1000 cells across the tube section, giving a mesh size in the core region of about 1 mm. The mesh size near the wall was progressively reduced down to 0.1 mm to enhance mesh resolution in this region of high velocity and temperature gradients. The quality of the mesh measured by its orthogonality and warpage was over 0.75, well above the generally accepted minimum value of 0.4 for a good mesh.

Other simulations were conducted using the same setup with 48 segments of the helical Kenics static mixer inserted to fill the whole tube, as illustrated in Figure 1(*d*). The mixer consists of left and right twisting helical elements with a standard length to diameter ratio of 1.5; detailed dimensions are given in Table 2. It should be noted that a mesh-independence study was conducted for each one of the flow geometries used. Very fine inflation layers of hexahedral cells were generated around the helical surfaces, so that the mesh was progressively reduced down to 0.15 mm at these surfaces and at the pipe wall to accurately capture the velocity and temperature gradients in these regions.

3.1.2 Boundary conditions

In all simulations, a uniform temperature T_{in} = 20 °C and a mass flowrate $\dot{m} = 0.0281$ kg s^{-1} were specified at the heating tube inlet, and a zero gauge pressure was set at the outlet. The mass flowrate was chosen to give a mean flow velocity $\overline{w} = 4.0$ cm s^{-1}, which is typical of values used in the processing of viscous food materials (Jung and Fryer, 1999; Steffe, 1996). A constant uniform wall temperature and a no-slip condition were assigned at the heating tube wall. In food processing, wall temperatures lower than 180 °C are usually used in practice; here, T_w was set at 140 °C. The temperature and velocity profiles at the exit of the heating tube were used as the inlet boundary conditions for the holding tube. In addition, the holding tube wall was specified as adiabatic with a no-slip condition, and a zero gauge pressure was set at the outlet. Where a static mixer was used, the helical surface was assumed adiabatic. For vibratory flow, the mesh displacement was specified using Eq. (2), and a harmonic velocity function defined by Eq. (3) was applied at the tube wall.

3.1.3 Numerical scheme

The CFD code uses a finite-volume-based method to discretise the governing transport Eqs. (4), (5), (6). In this method, the variable value at an integration point, ϕ_{ip}, is calculated from the variable value at the upwind node, ϕ_{up}, and the variable gradient, $\nabla\phi$, thus:

$$\phi_{ip} = \phi_{up} + \beta\nabla\phi\Delta\boldsymbol{r} \tag{12}$$

where β is a blend factor and $\Delta\boldsymbol{r}$ is the vector from the upwind node to the integration point. With β = 0, the scheme is first order accurate and does not result in non-physical variable values. On the other hand, with β = 1, the scheme is second order accurate but it may result in non-physical values. In the so-called 'High

Resolution Advection Scheme' implemented here, the value of β is calculated locally to be as close to 1 as possible without resulting in non-physical variable values (Barth and Jesperson, 1989). This scheme is therefore intended to satisfy the requirements of both accuracy and boundedness.

Simulations involving steady flow were conducted in the steady-state mode, whereas simulations of vibrational flow were conducted in the transient mode. For a transversely moving boundary, the mesh deformation option in CFX was used which allows the specification of the motion of nodes on boundary regions of the mesh. The motion of all remaining nodes is determined by the so-called displacement diffusion model which is designed to preserve the relative mesh distribution of the initial mesh.

The transient scheme used for the solution to march in time was the 'Second Order Backward Euler Scheme'. The simulation was solved over the entire mean residence time of the fluid which is determined by the tube length and mean flow velocity. For example, for a tube length of 2400 mm and flow velocity of 4.0 cm s^{-1}, as used here, the mean fluid residence time in the tube is 60 s. This time duration was divided into equal time steps, the size of which (1.6667×10^{-3} s) was determined by dividing the vibration cycle into an optimised number of 12 equal time steps. Using a larger number of time steps per vibration cycle did not change the simulation results but prolonged the simulations considerably. Smaller time steps were also tested but did not produce any significant improvement in results, however, the computational cost was dramatically increased.

Convergence of the numerical solution was assumed when the root mean squares (RMS) of the residuals of mass, momentum and energy all reached 10^{-4} at each time step which is a good level of accuracy given the complexity of the problem. Achieving this level of convergence typically required 8-12 iterations per time step for vibrational flow and about 50 iterations for steady flow. In practice, however, most of the equations generally reached residual RMS values well below the specified target.

3.2 Sterility and quality profiles: Lagrangian particle tracking

In a continuous flow process, different fluid elements will have different thermal histories and will be subjected to different levels of microbial lethality. To calculate local values of sterility at the exit, a Lagragian particle tracking method was used. Thus, the function of one-way coupled particle tracking was implemented in the CFD code to predict fluid trajectories along the tube. Unlike two-way coupling (i.e. full coupling) which takes into account not only the effect of particles on continuous phase flow but also the influence of continuous phase flow on particles, one-way coupling simply predicts the particles' path lines as a post-process based on the computed flow field (Mostofa et al., 2010). One-way coupling does not allow particles to affect continuous phase flow and therefore gives a much more accurate tracking of fluid flow than full coupling. Thus, massless microscopic fluid particles (1 μm) particles were introduced at the tube inlet and their trajectories and, hence, their temperature and velocity histories, were recorded. Thus, these massless particles are assumed to faithfully track the motion of the microorganisms and their temperature history. In the case of vibrated flow, because of the harmonic motion of the tube wall, some particles near the wall may move outside the numerical domain and are, therefore, ignored by the solver. In addition, some fluid particles become trapped in the slow moving fluid in the boundary layer and, thus, acquire extremely low velocities and do not reach the exit by the end of the simulation. In other words, some numerical leaking of particles is unavoidable despite using a small time-step.

In order to ensure that in vibrated flow a sufficient number of fluid particles were successfully tracked so that the flow field could be completely mapped, a large number (10^4) of such particles were introduced. The temperature and velocity histories of such particles were then used to calculate the sterility and quality profiles along the tube using a MATLAB code.

4. Validation of computational model

Though CFX is a generally well validated code as it is widely used, the computational work reported here was further validated where possible either by comparing results with theoretical solutions or experimental data where possible. The intention here was to try and validate the CFD model as much as possible so as to maximise confidence in the numerical results. The various stages of the validation process are described below.

The modelling by CFD of non-Newtonian power-law fluids flow under forced vibration without heat transfer was reported and experimentally validated in our previous studies (Deshpande and Barigou, 2001; Eesa and Barigou, 2008). Comparison with experiment showed that CFD is able to predict such complex flows with a very good accuracy within approximately ±10%, under a wide range of vibration conditions. We have also reported in our recent work (Tian and Barigou, 2015) detailed theoretical as well as experimental validations of temperature and heat transfer predictions in: (i) steady flow through a straight tube with wall heat transfer, of a Newtonian fluid with temperature-independent and with temperature-dependent viscosity; (ii) steady flow through a straight tube with wall heat transfer, of a non-Newtonian power-law fluid with temperature-independent viscosity.

Here, we validate our predictions of temperature against the classic analytical solution (Jakob, 1949) for the laminar flow of an isoviscous (i.e. temperature-independent viscosity) single-phase Newtonian fluid through a straight heating tube, and compare them to simulation results from Jung and Fryer (1999) executed with a different code (FIDAP), for the process conditions shown in Table 3. Both sets of simulations show excellent agreement with theory in Figure 3. We then validate our predictions of sterility and quality in the same heating tube against simulation results from Jung and Fryer (1999). The axial sterility and quality profiles along the tube are compared in Figure 4, showing excellent agreement between the two simulations.

There are, however, no experimental data available on the temperature profile in flows with heat transfer when subject to vibration. Nonetheless, given the excellent agreement of our CFD predictions of flow and heat transfer characteristics with theory and experimental results in all the above stages of the validation process, in addition to the excellent agreement of our food sterility and quality predictions to simulation results from Jung and Fryer (1999), we believe that the present CFD model is sufficiently robust and reliable for the purposes of studying the effects of vibration on the thermal processing of viscous fluids.

5. RESULTS AND DISCUSSION

In this work, we consider four tube flow configurations, as shown in Figure 1: (i) steady flow through a straight tube as used in a conventional sterilization process (**SF**); (ii) steady flow through a straight tube fitted along its whole length with a Kenics static mixer (**SF-KM**); (iii) steady flow through a straight tube with superimposed

transverse oscillations (**VF**); and (iv) steady flow through a straight tube subjected to transverse oscillations with angular step rotation of oscillation orientation (**VF-SR**).

5.1 Effect of vibration on radial temperature profile

The radial temperature contours obtained at the tube exit under vibration are compared to the steady-state contours with and without a Kenics static mixer in Figure 5. The volume-flowrate weighted mean temperature is calculated using Eq. (10) with T in lieu of F, and the axial profiles of $\overline{T}$ are compared in Figure 6.

In steady laminar flow (**SF**), heat is transferred radially by conduction; therefore, in this relatively short tube (L = 2.4 m), only fluid flowing near the tube wall is significantly heated whereas the vast majority of the fluid remains at more or less the inlet temperature. Heating of the inner parts of the flow is a very slow process and significant levels can only be achieved in long tubelines. The Kenics static mixer (**SF-KM**) produces substantially improved radial and axial temperature profiles, but results are considerably inferior to those provided by vibratory flow. In addition, the Kenics mixer caused a much higher pressure drop than steady flow or flow with vibration (about six to seven folds).

The velocity vector distributions in Figure 5 show that, whilst in steady flow there is little or no radial fluid motion, under vibration a secondary radial flow is superimposed on the main axial flow, which is much more vigorous than that generated by the Kenics mixer. The presence of strong vortical structures is clearly apparent generating a spiralling fluid motion along the tube. This secondary flow which introduces a significant chaotic advection flow, causes continuous radial mixing with hot fluid flowing from the tube wall to the centre and back in four spiralling loops, thus, generating a strong degree of radial convection which results in the quasi-uniform temperature profiles observed across the tube. This radial flow increases in strength as vibration intensifies (data not shown). In this case, the mean resultant velocity in the radial plane, $\overline{u}$, is ~ zero for **SF**, ~ 2.1 cm s^{-1} for **SF-KM**, and ~ 1.1 cm s^{-1} for **VF** and **VF-SR**. Even though $\overline{u}$ is larger for the Kenics mixer, the secondary flow generated has a strong rotational component which is not as effective for radial mixing as the flow generated by the wall oscillations.

A four-fold enhancement in wall heat transfer was also observed, which is attributed primarily to the disruption of the thermal boundary layer caused by the swirling fluid motion induced by vorticity. These effects depend on the intensity of vibration and the rheology of the fluid; more viscous fluids require a more energetic vibration but the effects appear to be more sensitive to the amplitude than the frequency of wall oscillations (Eesa and Barigou, 2010).

Simple transverse oscillations (**VF**), however, produce four salient vortices which trap cold fluid inside, hamper radial mixing and reduce temperature uniformity. When angular step changes in the plane of oscillation are imposed (**VF-SR**), the vortex centres are made to move around, hence, causing cold fluid inside these regions to mix with hotter fluid flowing inwards from the wall, and a much improved temperature profile results in both radial (Figure 5) and axial (Figure 6) directions. The value of the step rotation frequency **Ω** is somewhat significant in achieving the highest mean temperature at the tube exit, the best temperature uniformity across radius and the best wall heat transfer coefficient. The optimum value of **Ω** is a function of the process

parameters. Numerical experiments within the range Ω = 0.067 – 0.2 Hz (i.e. Δt = 5 – 15 s), revealed a maximum difference of ~ 5 °C in mean exit temperature. However, sterility and quality calculations introduce further sensitivities because of their exponential form and so, even small differences in temperature can translate into much more significant differences in the F-value and C-value. Optimum conditions can in practice be determined by adjusting the value of Ω upwards from zero until the cold vortex regions fade, a process which may require a certain amount of trial and error.

It should be noted that in this work amplitude and frequency have been kept deliberately low to demonstrate that the principle works at easily manageable levels of vibration intensity. If higher vibration intensities are used, these should lead to even stronger effects (up to some limit). Optimum vibration conditions (amplitude and frequency) will depend on a number of factors including fluid rheology and physical properties, flowrate, tube diameter, wall and inlet temperatures. Some numerical experimentation is required to determine such conditions for a given situation. Here, we selected parameters such as fluid viscosity, temperatures, tube length, diameter etc. which represent a realistic industrial situation, but at the same time did not make the computations too costly. A detailed parametric study of the problem would require numerous simulations. As the main purpose of our current investigation is to demonstrate the benefits of this chaotic advection technique for continuous food sterilisation, such a detailed study is beyond the scope of this paper.

5.2 Effect of vibration on thermal boundary layer

Results show that transverse oscillations greatly affect thermal boundary layer development, as depicted in Figure 7. In steady flow, the azimuthally-averaged axial temperature profile shows little change over the whole tube length as the thermal boundary layer develops extremely slowly. With the Kenics mixer fitted, the situation improves considerably. Under **VF-SR**, however, the thermal entrance length (~ 0.9 m) is dramatically reduced by an order of magnitude compared to the steady state (~ 11 m), with **VF-SR** being clearly superior to **VF**. This further confirms that the full effects of the oscillations are felt in the early stages of the flow and, consequently, the tube length required for a given thermal process could be greatly reduced. These effects are also captured in Figure 6 showing the fast and substantial rise in mean fluid temperature along the tube generated by vibratory flow compared to steady flow with and without a static mixer.

5.3 Effect of vibration on food sterility

In a safe sterilisation process, all of the fluid must receive the required minimum level of sterilisation. The fluid flowing along the tube centreline, being the fastest, is the slowest to reach such a level of sterility. This situation is much worse for viscous fluids flowing in the laminar regime. The challenge facing any continuous process of this kind, therefore, is to ensure that the fluid at the centre is safe without overcooking too much the slow moving fluid near the hot tube wall. Low acid foods with a sterility value greater than 2.52 min are usually considered safe. Such a value is based on the lethality of the organism *Clostridium botulinum*, but in practice many pathogens are more heat resistant and F-values of 5 – 12 min are typically used (Steffe and Daubert, 2006). Such F-values usually require extremely long processing tubes which can run into hundreds of metres (Jung and Fryer, 1999).

The radial temperature history profiles obtained by CFD (Figure 5) were used to compute the radial sterility distributions across the exit section of the heating tube using the Lagrangian particle tracking algorithm described above. In these calculations, the thin (1 mm) region adjacent to the hot wall, where fluid velocity is very small, was ignored as it contains extremely large F-values (in this region F tends to infinity). Contours of the radial distribution of sterility at the exit section of the heating tube are shown in Figure 8 for the four flow regimes studied. The transverse oscillations and the Kenics mixer introduce a certain degree of asymmetry in the sterility distribution around the tube axis. Consequently, the tube cross-section was divided into 15 shells of equal width and an azimuthally averaged F-value was calculated to represent each shell. Thus, azimuthally-averaged radial sterility profiles were obtained at the tube exit and are compared in Figure 9.

In steady flow $F \ll 10^{-2}$ over about 80% of the tube radius, and increases exponentially towards the wall reaching extremely high values, many orders of magnitude greater than the value at the centre (hence the use of a log scale). Due to better radial mixing, the outer wall region where F rises steeply is much narrower for the other three flow regimes, thus strongly diminishing its impact on the heat treatment of the fluid. The **VF-SR** technique produces the highest local F values and, as shown in Table 4, the mean sterility $\bar{F}_{VF-SR}$ is much greater than for the other flow regimes ($117.5 \times \bar{F}_{SF}$; $21.7 \times \bar{F}_{SF-KM}$; $5.3 \times \bar{F}_{VF}$). The uniformity of the radial F distribution across the tube section is also the best ($C_{v\text{-}F} \sim 1.09$), significantly better than for **VF** ($C_{v\text{-}F} \sim 1.33$) and substantially better than for **SF-KM** ($C_{v\text{-}F} \sim 1.58$) and **SF** ($C_{v\text{-}F} \sim 3.75$). As a result of the remarkable radial uniformity of sterility achieved by **VF-SR**, the mean value $\bar{F}$ across the tube, is close to the local F values; in particular, the ratio of $\bar{F}$ to F_c, the value at the centre, which is conventionally regarded as the coldest point, is ~ 1.0 (note in vibrated flow the coldest point is not located at the centre); in steady flow, however, $\bar{F} \sim 8{\times}10^{7} \times F_c$. The static mixer shows segregation areas of very low F-values and the four cold vortex regions are also apparent in the **VF** contours as regions of low sterility (Figure 8), but this regime still outperforms the **SF-KM** configuration, yielding a mean F-value which is several times greater (Table 4).

As the fluid flows in parallel layers with little/no radial mixing, $\bar{F}$ is clearly not a reliable measure of sterility in steady flow, so that high mean values do not necessarily imply a safe level of sterility because of the lack of uniformity. Even with the Kenics mixer the temperature history along the tube results in many scattered pockets where the local F-value is ~ 20 times smaller than $\bar{F}$. The use of an average F-value is, however, much more justifiable in a radially well-mixed flow such as the vibrated flow (**VF-SR**) considered here, where chaotic advection ensures that fluid elements continuously exchange radial position along the tube, thus, narrowing the residence time distribution substantially, as shown in Figure 10, and consequently the radial temperature and sterility distributions.

There is also a huge difference between the four regimes of flow in the axial growth of the mean F-value, as shown in Figure 11. In steady flow and in steady flow with Kenics mixer, F rises relatively very slowly along the tube. Under vibration, however, radial mixing ensures that the fluid at the tube centre is heated much more rapidly, thus causing F to grow exponentially rapidly with z; the effect is much more pronounced for **VF-SR** than for **VF**, however. Thus, it follows that a given level of mean sterility can be achieved in much shorter tubes when flow is vibrated. For example, for the process conditions considered here, as shown in Figure 12,

achieving the mean sterility value of 37.6 s obtained with **VF-SR** in the 2.4 m long tube, would require a heater which has a length of ~ 7.7 m with **SF**, ~ 3.8m with **SF-KM** and ~ 2.9 m with **VF**.

However, as pointed out earlier, it is important to note that the use of mean temperature and mean sterility can be seriously misleading. Indeed, any assessment or comparison should be made on the basis of the minimum sterility value attained in the flow. For the case represented in Figure 12, the minimum sterility achieved in the **VF-SR** tube which is 2.4 m long is F_{min} = 12.5 s. To achieve this minimum value, simulations yielded tube lengths of approximately 26.0 m for **SF**, 4.0 m for **SF-KM** and 3.2 m for **VF**.

5.4 Effects of vibration on food quality

For a given level of sterility, the aim is to minimise food quality loss, i.e. the C-value defined above in Eq. (8), to preserve nutritional value. Thus, comparison of quality loss is only meaningful when based on equal sterility. Initially, we make such a comparison on the basis of equal $\bar{F}$ and then on the basis of equal F_{min}.

Contours of the radial distribution of quality for the four flow regimes studied are compared in Figure 13, for a given mean sterility $\bar{F}$ = 37.6 s, which is the value achieved by **VF-SR** at the exit of the 2.4 m tube. As discussed above, to achieve this same mean sterility value longer tubes are required for **SF**, **SF-KM** and **VF** (Figure 12). The corresponding radial profiles of azimuthally-averaged C-value in these tubes are also plotted in Figure 14. Clearly, **VF-SR** produces by far the lowest C-values and the most uniform profile ($C_{v\text{-}C}$ values are given in Table 5), outperforming by far the traditional steady flow process as well as the Kenics mixer. The axial profiles of the mean C-value depicted in Figure 15 show that, for a given $\bar{F}$, the **VF-SR** technique produces a much lower average quality loss compared to **SF** and **SF-KM**.

Again a comparison on the basis of the minimum sterility value F_{min} = 12.5 s for **VF-SR**, shows that the longer tube lengths needed for the other flow configurations discussed above (i.e. 26.0 m for **SF**, 4.0 m for **SF-KM** and 3.2 m for **VF**) cause even much larger losses of food quality: $\bar{C}$ = 169.4 s for **SF**, 47.5 s for **SF-KM** and 38.4 s for **VF**.

These results were obtained using z_C = 48 °C for thiamine denaturation, as stated in Section 2.4. However, values quoted in the literature lie in the range 30 – 50 °C. Therefore, a sensitivity analysis using z_C values of 30 °C and 40 °C, was conducted. Contours and profiles of the C-value were obtained which are closely similar to those depicted in Figures 13 – 15 for z_C = 48 °C. The uniformity of the radial distribution of the local C-value for each flow configuration improved significantly as z_C increased, i.e. the $C_{v\text{-}C}$ value decreased by ~ 20% for **VF-SR** and **VF**, and by ~ 25% for **SF** and ~ 40% for **SF-KM**. The axial profiles of the mean quality led to different values of $\bar{C}$ at the tube exit, as shown in Figure 15. Such a profile is only moderately affected by z_C in the case of vibrated flow (~ 10 – 15%), but is considerably affected in the case of steady flow and steady flow with a Kenics mixer (~ 25%). However, for a given value of z_C results afforded by the vibration technique are far superior to those of conventional processing even when a static mixer is used.

5.5 Vibration in the context of a heat-hold-cool system

Industrial processes do not aim to achieve the required level of food sterility in the heating tube. In continuous aseptic processing, a heat-hold-cool system is normally used. There is a clear quality advantage in in-flow sterilisation at higher temperatures and for shorter times i.e. HTST, because the activation energy for the reactions which cause microbial destruction, i.e. sterility, are higher than those which result in quality loss (Holdsworth, 1992). Sterilisation reactions proceed ~100 times faster than loss of quality reactions. Therefore, compared to in-can processing the time needed for sterilisation is reduced and the amount of quality loss is also reduced (Hallstrom et al., 1988).

HTST processes involve heating to the required sterilisation temperature, holding the product at such a temperature for long enough to ensure sufficient pathogen spore destruction, and then cooling to packaging temperature. In practice, to ensure product safety, the length of the holding tube is usually calculated based on the assumption of Newtonian laminar flow with all of the fluid flowing at the centreline maximum velocity, i.e. twice the mean velocity. Inevitably, such a conservative approach leads to very long holding tubes on the order of hundreds of metres, and very long residence times, thus, contradicting the HTST assumption and producing food of poor quality.

The results discussed above have shown that **VF-SR** can achieve much higher $\bar{F}$ values in a relatively short tube compared with **SF** (~ 117 folds in a 2.4 m tube, see Table 4). It should be noted that in a conventional steady-state process, relatively little lethality is accumulated in the heater, and most of the sterility is achieved in the holding tube. However, given the fast rise in temperature accompanied by the fast rise in F achieved by the **VF-SR** technique in the heater, a holding stage may not be necessary. This represents an additional significant improvement in the sterilization process. In cases where higher $\bar{F}$ values are required at the exit of the heating stage, a longer vibrated heating tube could be used. The exponential variation of $\bar{F}$ with z, shown in Figure 11, indicates that a large increase in $\bar{F}$ could be achieved through only a relatively small increase in tube length. However, we need to assess whether an increase in $\bar{F}$ is better achieved by using a longer vibrated heater or by using a holding tube instead.

The axial profiles of mean sterility in the heating tube and holding tube are shown in Figure 16. An average sterility value of 37.6 s is reached at the end of the heating stage. Adding a holding tube of 2.4 m length yields a total average sterility of ~ 250 s. The same value could be achieved by extending the **VF-SR** heating tube by only an extra ~ 0.6 m. At the same time, the associated increase in the mean C-value would be ~ 78 s for the holding tube and ~ 32 s for the extended heater; i.e. a relatively short extension of the heater achieves the same mean sterility with a much reduced loss of quality.

The advantages of extending the vibrated heating tube over using a holding tube become even more striking when comparing on the basis of minimum sterility. Using a holding tube of 2.4 m length will increase F_{min} from 12.5 s at the exit of the heater to ~ 190.9 s with the corresponding exit mean C-value rising from 26.5 s to 104.9 s. In contrast, computations show that this same minimum sterility could be achieved by extending the heating tube by only ~ 0.43 m, with an accumulated average quality at exit of 48.5 s. Therefore, it can be clearly seen that a heating tube extension of 0.43 m would increase the minimum level of sterility by 178.4 s , the same as a holding tube of 2.4 m length, but with much less loss of quality (22 s compared with 78.4 s). These results demonstrate that there are considerable benefits in using an extended heater and that for most

applications a holding stage may not be necessary if a **VF-SR** heater is used.

The cooler gives the opposite scenario to the heater. In a normal steady flow process, the cooling stage tends to contribute some additional lethality and, hence, causes some additional quality loss as the material cools at a finite rate. Thus, the aim is to cool at the fastest rate possible to preserve as much of the product quality as possible. The wall is maintained at a low temperature and peripheral fluid in this region cools rapidly, whilst at the centre the temperature of the fluid continues to rise slowly over a considerable length of tubing before responding to the cooling effect. In a cooling tube, vibration would be expected to produce similar desirable effects to those observed in the heater, i.e. significant radial mixing resulting in enhanced heat transfer at the wall, a nearly uniform radial temperature distribution, and much shorter cooling tubes compared to the steady-state configuration with or without the inclusion of a static mixer. Detailed simulations of a complete heat-hold-process are beyond the scope of this paper and will be the subject of a further study.

6. CONCLUSIONS

The superimposition of a forced lateral vibration produces a secondary chaotic advection flow which causes significant radial fluid mixing. In a heating tube with an isothermal wall, this leads to a nearly uniform radial temperature profile, a rapid development in the thermal boundary layer, and a several-fold increase in radial heat transfer. These effects are governed by a number of factors including, the intensity of vibration, viscosity (and more generally rheology) of the fluid, material throughput, wall temperature and tube diameter.

The case study presented here shows that when vibration is used, high sterility levels can be achieved in relatively short heating tubes. The disruption of the thermal boundary layer lowers the temperature in the wall region, thus, greatly reducing overcooking of the product. Because of the radial mixing induced, the fluid also receives a nearly uniform heat treatment, so that product quality loss is minimised compared to conventional steady flow with or without the use of a Kenics static mixer. The combination of these benefits suggests that the use of a holding tube in a traditional heat-hold-cool process can be avoided in a vibrated process and the whole process could be made much shorter. Vibration, therefore, seems to create processing conditions that are much more in agreement with the HTST assumption which is often contradicted in conventional steady flow processing.

Acknowledgements

Shuai Tian's PhD research was funded by a China Government & University of Birmingham scholarship.

NOMENCLATURE

A	Vibration amplitude, m
C	Quality value, s
$\bar{C}$	Volume-flowrate weighted mean quality value, s
C_p	Specific heat capacity, J kg^{-1} K^{-1}
$C_{v\text{-}C}$	Coefficient of variation of quality value, (-)
$C_{v\text{-}F}$	Coefficient of variation of sterility value, (-)
E_a	Activation energy for viscosity, J mol^{-1}

562 F Local sterility value, s
563 F_{min} Minimum sterility value, s
564 $\bar{F}$ Volume-flowrate weighted mean sterility value, s
565 f Vibration frequency, Hz
566 k_0 Pre-exponential factor, Pa s
567 L Tube length, m
568 r Radial position, m
569 R Tube radius, m
570 R_g Gas constant, J mol^{-1} K^{-1}
571 t Time, s
572 Δt Time interval of angular step rotation, s
573 T Temperature, °C
574 T_{in} Inlet temperature, °C
575 $\bar{T}$ Volume-flowrate weighted mean temperature, °C
576 T_w Wall temperature, °C
577 $\bar{u}_{xy}$ Mean resultant velocity in radial plane, m s^{-1}
578 w Axial velocity, m s^{-1}
579 $\overline{w}$ Mean axial velocity, m s^{-1}
580 x Wall displacement, m
581 z Axial position, m
582
583 *Greek symbols*
584 μ Temperature-dependent viscosity of Newtonian fluid, Pa s
585 ρ Density, kg m^{-3}
586 λ Thermal conductivity, W m^{-1} K^{-1}
587 ω Angular vibration frequency, rad s^{-1}
588 Ω Frequency of step rotation of oscillation orientation, Hz
589

590 **REFERENCES**

591 Aref, H., 1984. Stirring by chaotic advection. J. Fluid Mech. 143, 1-21.

592 Aref, H., 1990. Chaotic advection of fluid particles. Philos. T. Roy. Soc. A., 333 (1631), 273-288.

593 Ball, C.O., Olson, F.C.W., 1957. Sterilization in food technology. Theory practice and calculations.
594 McGraw-Hill Book Co., New York.

595 Barth, T.J., Jesperson, D.C., 1989. The design and application of upwind schemes on unstructured meshes.
596 AIAA, pp. 1-12 [AIAA, paper 89-0366].

597 Bird, R.B., Armstrong, R.C., Hassager, O., Curtiss, C.F., 1987. Dynamics of Polymeric Liquids: Fluid
598 Mechanics, second Ed, Vol. 1. John Wiley, New York.

599 Chagny, C., Castelain, C., Peerhossaini, H., 2000. Chaotic heat transfer for heat exchanger design and
600 comparison with a regular regime for a large range of Reynolds numbers. Appl. Therm. Eng. 20 (17),
601 1615-1648.

602 Deshpande, N.S., Barigou, M., 2001. Vibrational flow of non-Newtonian fluids. Chem. Eng. Sci. 56 (12),
603 3845-3853.

604 Eesa, M., Barigou, M., 2008. CFD analysis of viscous non-Newtonian flow under the influence of a
605 superimposed rotational vibration. Comput. Fluids 37 (1), 24-34.

606 Eesa, M., Barigou, M., 2010. Enhancing radial temperature uniformity and boundary layer development in
607 viscous Newtonian and non-Newtonian flow by transverse oscillations: a CFD study. Chem. Eng. Sci. 65 (6),
608 2199–2212.

609 Eesa, M., Barigou, M., 2011. CFD simulation of transverse vibration effects on radial temperature profile and
610 thermal entrance length in laminar flow. AIChE J. 57 (1), 51–56.

611 Gundogdu, M.Y., Carpinlioglu, M.O., 1999. Present state of art on pulsatile flow theory – (Part 1: Laminar and
612 transitional flow regimes). JSME Int. J. Ser. B. 42 (3), 384-397.

613 Hallström, B., Skjöldebrand, C., Trägârdh, C., 1988. Heat transfer and food products. Elsevier Applied Science,
614 London.

615 Hobbs, D.M., Muzzio, F.J., 1997. The Kenics static mixer: a three-dimensional chaotic flow. Chem. Eng. J. 67
616 (3), 153-166.

617 Holdsworth, S.D., 1992. Aseptic processing and packaging of food products. Elsevier Applied Science, London.

618 Hui, Y.H., 2006. Handbook of food science, technology, and engineering, vol 3. CRC Press, Taylor & Francis
619 Group, Boca Raton, FL.
620
621 Jakob, M., 1949. Heat transfer. Wiley, New York.

622 Jung, A., Fryer, P.J., 1999. Optimising the quality of safe food: Computational modelling of a continuous
623 sterilisation process. Chem. Eng. Sci. 54 (6), 717-730.

624 Klaczak, A., 1997. Report from experiments on heat transfer by forced vibrations of exchangers. Heat Mass
625 Transfer 32 (6), 477-480.

626 Lee, Y.H., Chang, S.H., 2003. The effect of vibration on critical heat flux in a vertical round tube. J. Nucl. Sci.
627 Technol. 40 (10), 734-743.

628 Mostofa, M.G., Kil, K., Hwan, A., 2010. Computational fluid analysis of abrasive water jet cutting head. J. Mech.
629 Sci. and Tech. 24 (1), 249-252.

630 Ottino, J.M., 1989. The kinematics of mixing: Stretching, chaos, and transport. Cambridge University Press,
631 Cambridge.

632 Saatdjian, E., Rodrigo, A.J.S., Mota, J.P.B., 2012. On chaotic advection in a static mixer. Chem. Eng. J. 187(0),
633 289-298.

634 Steffe, J.F., Daubert, C.R., 2006. Bioprocessing tubelines: Rheology and analysis. Freeman Press, East Lansing,
635 Michigan.

636 Steffe, J.F., 1996. Rheological Methods in Food Process Engineering, second Ed. Freeman Press, East Lansing,
637 Michigan.

638 Tian, S., Barigou, M., 2015. An improved vibration technique for enhancing temperature uniformity and heat
639 transfer in viscous fluid flow. Chem. Eng. Sci. 123, 609-619.

FIGURE AND TABLE CAPTIONS

Figure 1. Flow configurations: (*a*) flow through a tube subjected to transverse oscillations (**VF**); (*b*) flow through a tube subjected to transverse oscillations with step rotation of vibration orientation (**VF-SR**); (*c*) steady flow through a tube (**SF**); (*d*) steady flow through a tube fitted with a Kenics static mixer (**SF-KM**), showing 4 elements out of 48.

Figure 2. Illustration of grid used on MATLAB for evaluation of volume-flowrate weighted mean temperature, sterility and quality over tube cross-section (total number of cells, N = 1860 cells).

Figure 3. Validation of CFD-predicted temperature profiles of an isoviscous fluid in steady-state flow in a heating tube against theory (Jakob, 1949) and simulation results from Jung & Fryer (1999), for the processing conditions of Table 3.

Figure 4. Validation of CFD-predicted axial profiles of sterility and quality of an isoviscous fluid in steady-state flow in a heating tube against simulation results from Jung & Fryer (1999), for the processing conditions of Table 3.

Figure 5. Radial temperature and velocity vector distributions at the exit section of the heating tube.

Figure 6. Axial profile of mean temperature in the heating tube.

Figure 7. Axial contour plot of azimuthally-averaged temperature in the heating tube: (*a*) **SF**; (*b*) **SF-KM**; (*c*) **VF**; (*d*) **VF-SR**.

Figure 8. Radial contour plot of F-value at the exit section of the heating tube.

Figure 9. Radial profile of azimuthally-averaged F-value at the exit section of the heating tube.

Figure 10. Fluid residence time distribution in the heating tube.

Figure 11. Axial profile of mean F-value in the heating tube.

Figure 12. Axial profile of mean F-value in heating tubes with different flow regimes achieving the same mean sterility ($\bar{F}$ = 37.6 s) at the exit section.

Figure 13. Radial contour plot of C-value at the exit section of heating tubes with different flow regimes achieving the same mean sterility ($\bar{F}$ = 37.6 s) at the exit section (note that the red colour in the **SF** plot is ~ four-fold greater than the top end of the scale).

Figure 14. Radial profile of azimuthally-averaged C-value at the exit section of heating tubes with different flow regimes achieving the same mean sterility ($\bar{F}$ = 37.6 s) at the exit section.

Figure 15. Axial profile of mean C-value in heating tubes with different flow regimes achieving the same mean sterility ($\bar{F}$ = 37.6 s) at the exit section.

Figure 16. Development of mean F-value along heating and holding tubes.

Table 1. Process parameters used in simulations.

Table 2. Dimensions of Kenics static mixer (Figure 1(*d*)).

Table 3. Process parameters used for CFD validation (Jung and Fryer, 1999).

Table 4. Mean sterility and quality in the heating tube (L = 2400 mm).

Table 5. Mean quality corresponding to the same mean sterility at exit ($\bar{F}$ = 37.6 s).

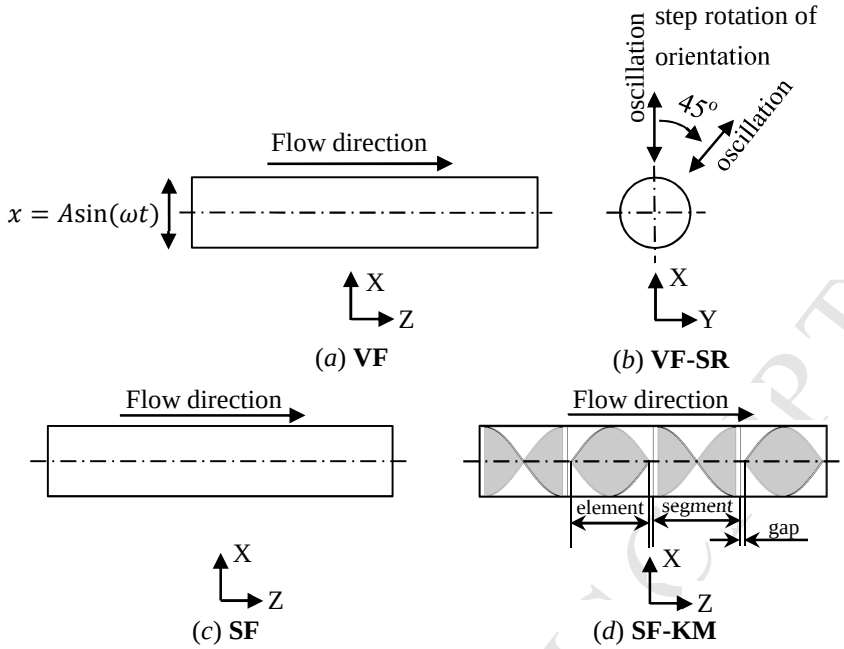

Figure 1. Flow configurations: (*a*) flow through a tube subjected to transverse oscillations (**VF**); (*b*) flow through a tube subjected to transverse oscillations with step rotation of vibration orientation (**VF-SR**); (*c*) steady flow through a tube (**SF**); (*d*) steady flow through a tube fitted with a Kenics static mixer (**SF-KM**), showing 4 elements out of 48.

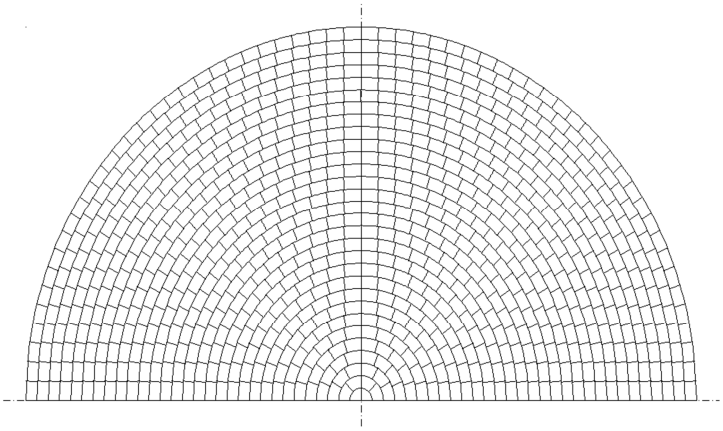

Figure 2. Illustration of grid used on MATLAB for evaluation of volume-flowrate weighted mean temperature, sterility and quality over tube cross-section (total number of cells, N = 1860 cells).

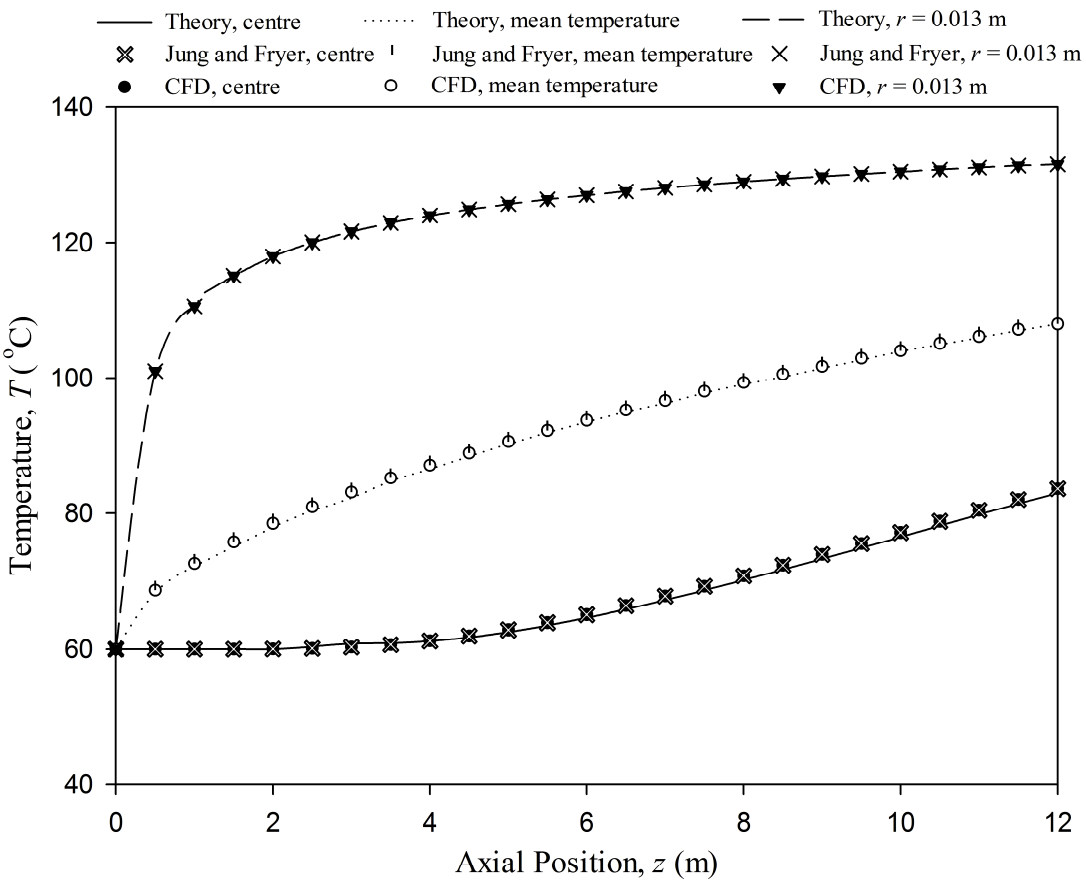

Figure 3. Validation of CFD-predicted temperature profiles of an isoviscous fluid in steady-state flow in a heating tube against theory (Jakob, 1949) and simulation results from Jung & Fryer (1999), for the processing conditions of Table 3.

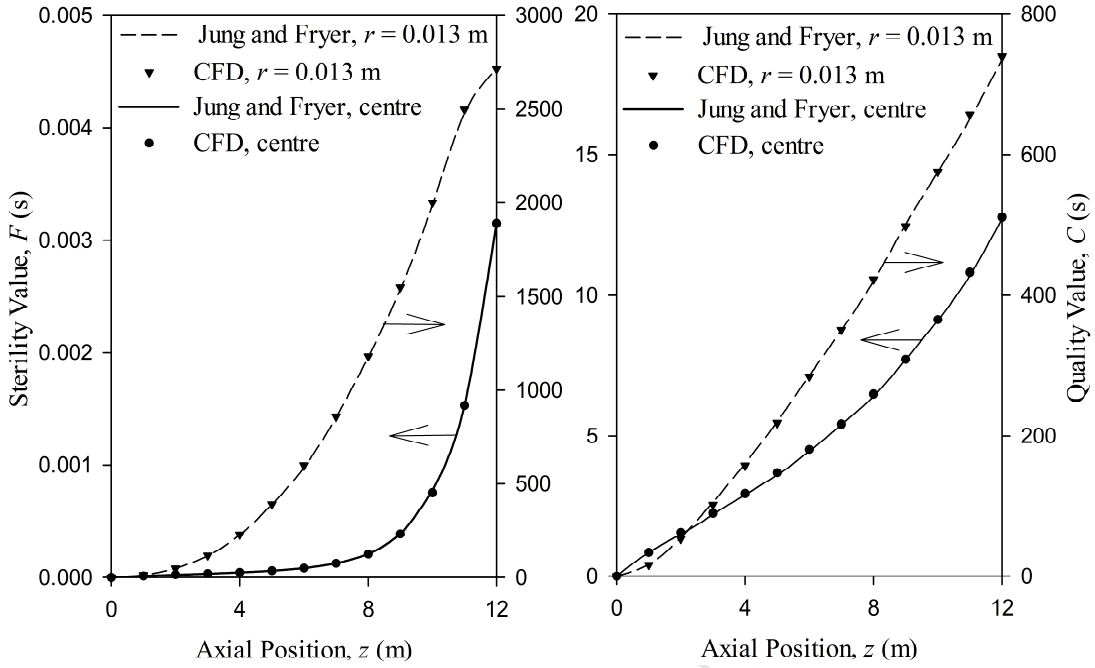

Figure 4. Validation of CFD-predicted axial profiles of sterility and quality of an isoviscous fluid in steady-state flow in a heating tube against simulation results from Jung & Fryer (1999), for the processing conditions of Table 3.

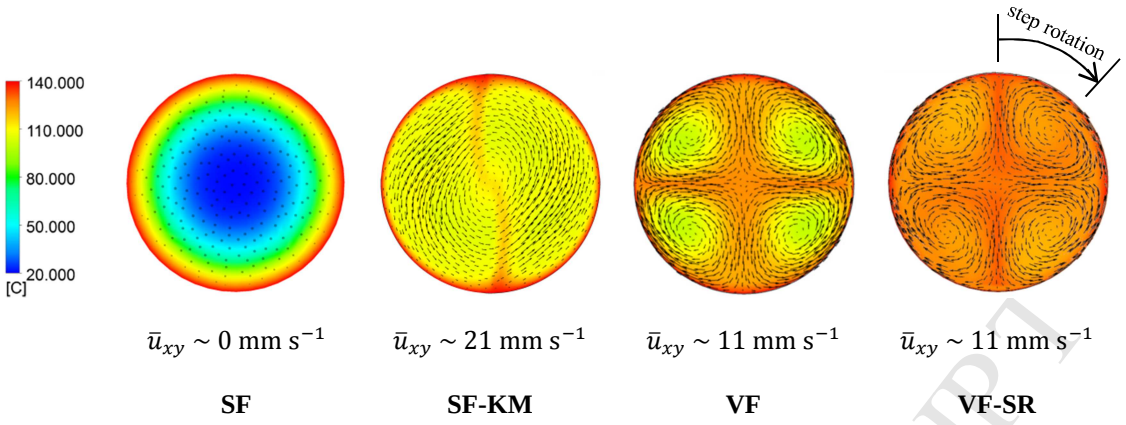

Figure 5. Radial temperature and velocity vector distributions at the exit section of the heating tube.

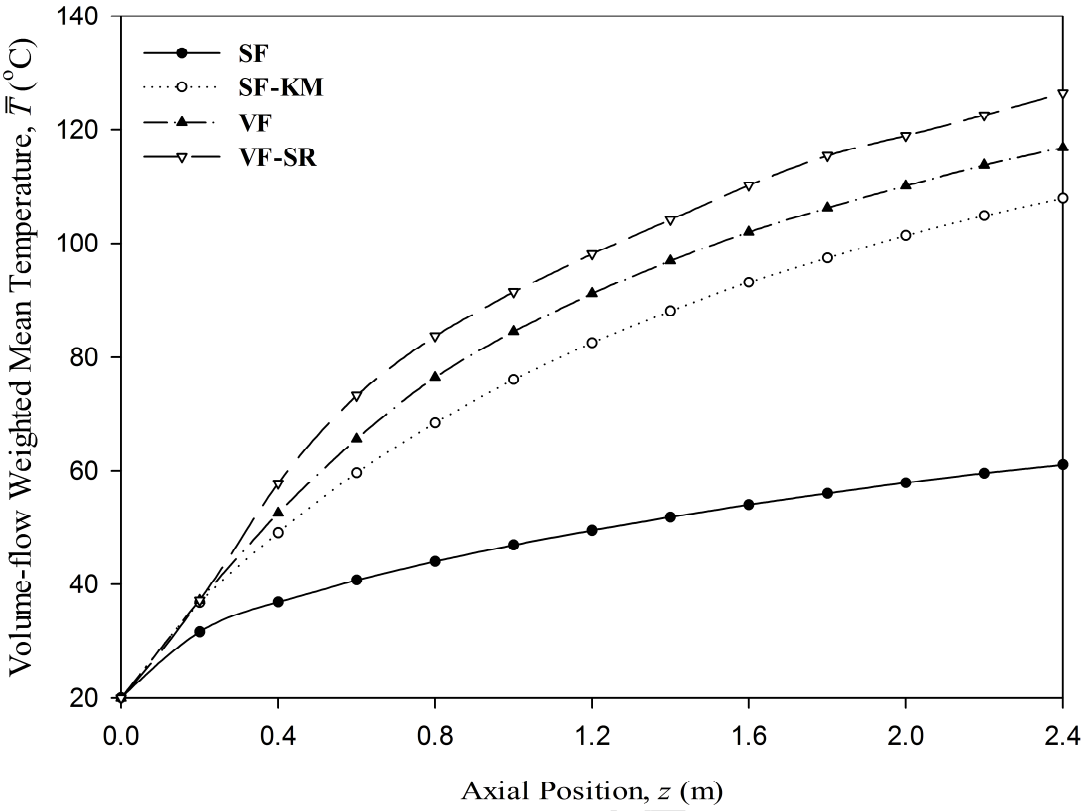

Figure 6. Axial profile of mean temperature in the heating tube.

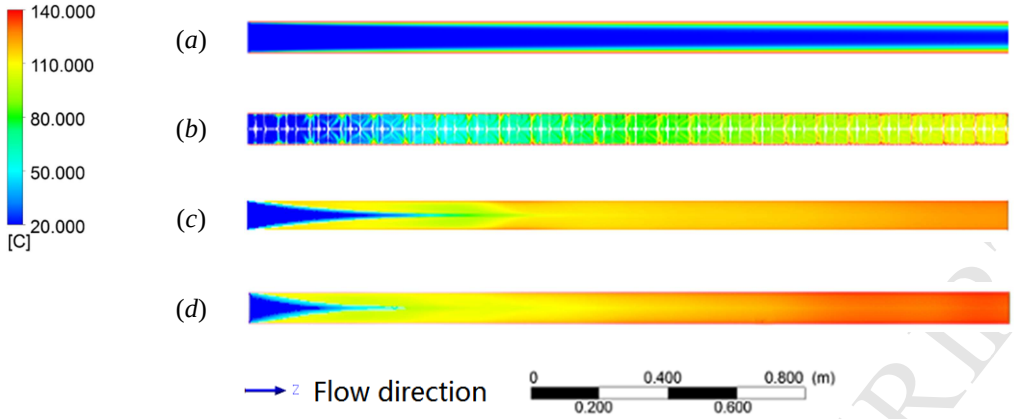

Figure 7. Axial contour plot of azimuthally-averaged temperature in the heating tube: (*a*) **SF**; (*b*) **SF-KM**; (*c*) **VF**; (*d*) **VF-SR**.

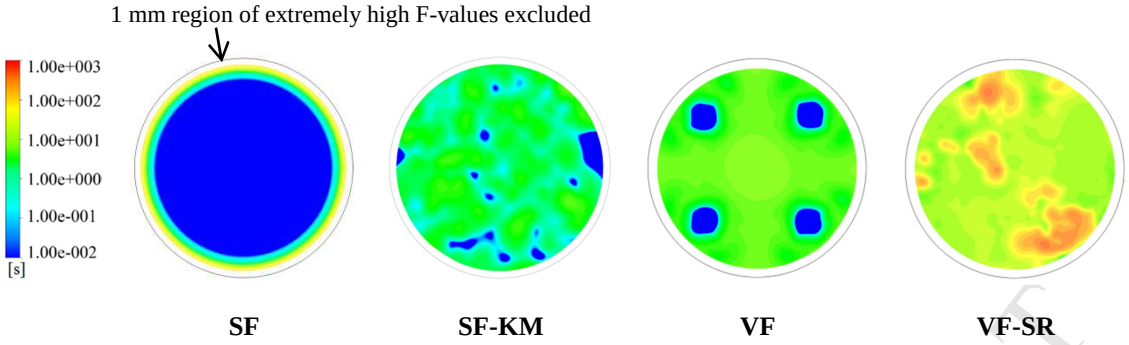

Figure 8. Radial contour plot of F-value at the exit section of the heating tube.

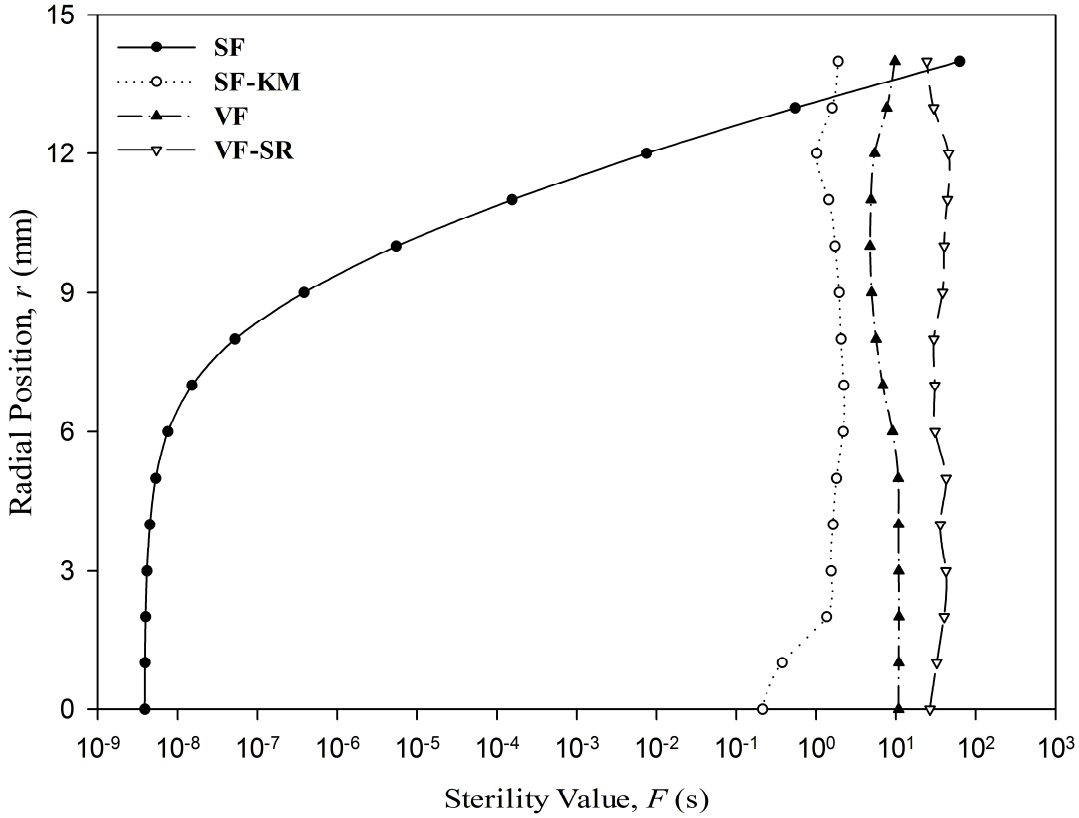

Figure 9. Radial profile of azimuthally-averaged F-value at the exit section of the heating tube.

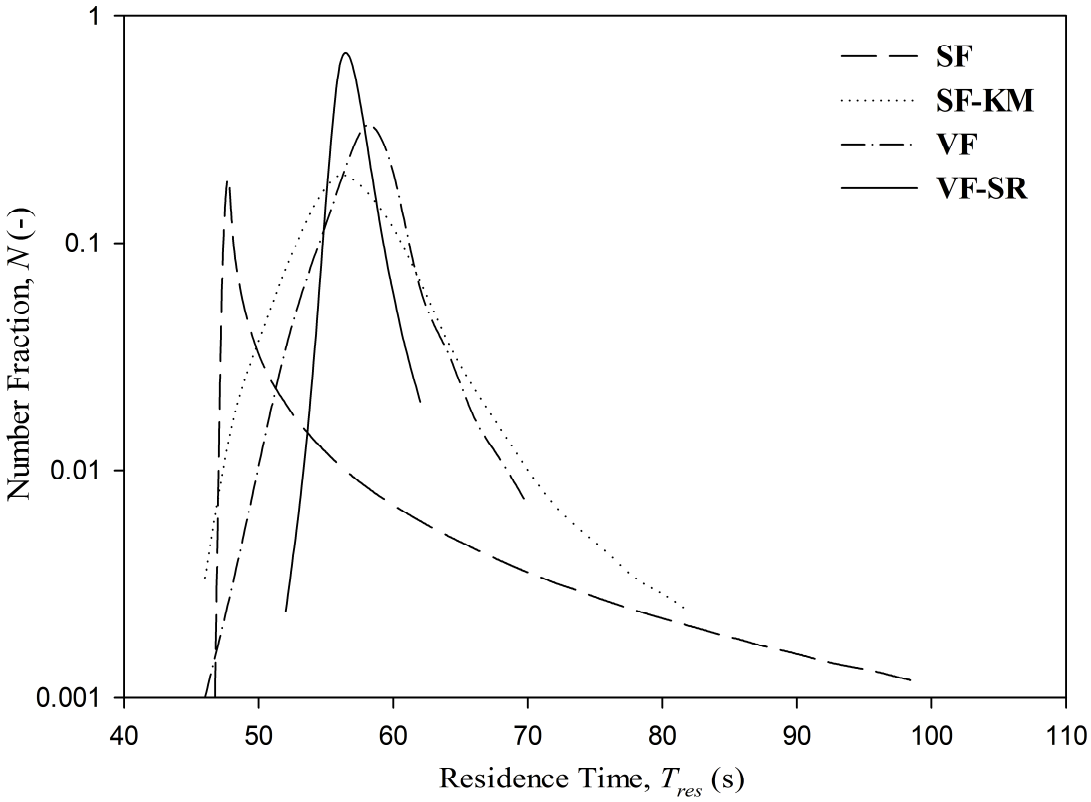

Figure 10. Fluid residence time distribution in the heating tube.

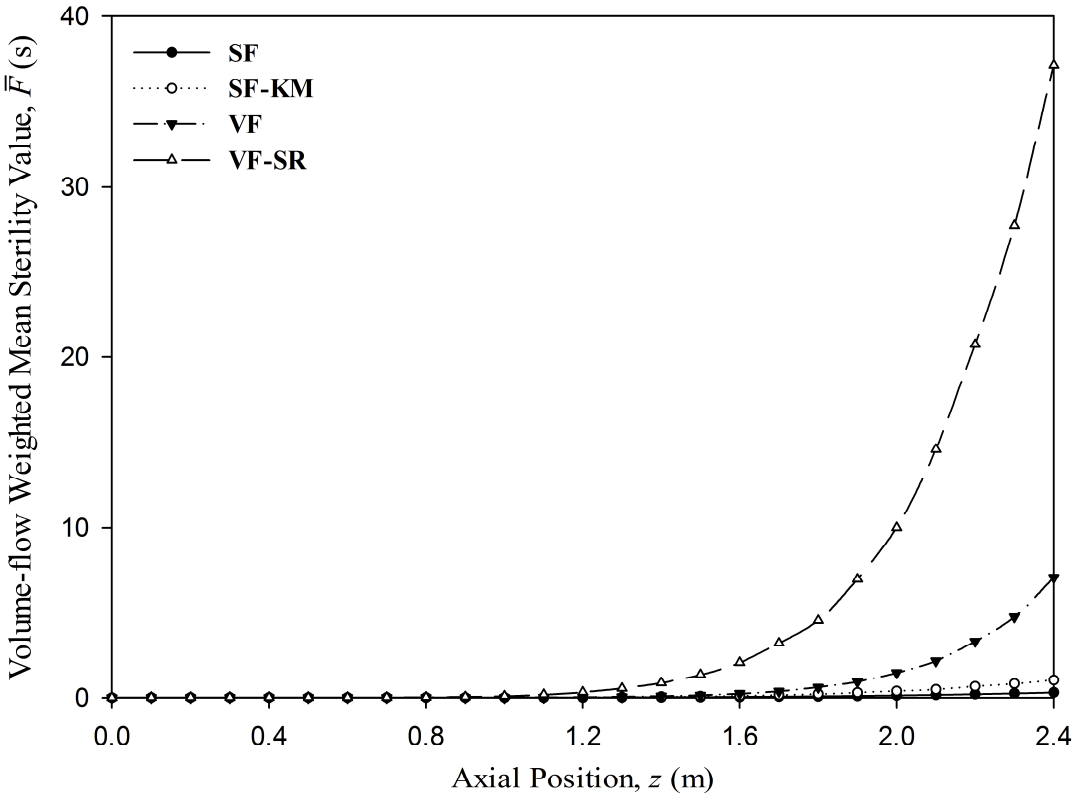

Figure 11. Axial profile of mean F-value in the heating tube.

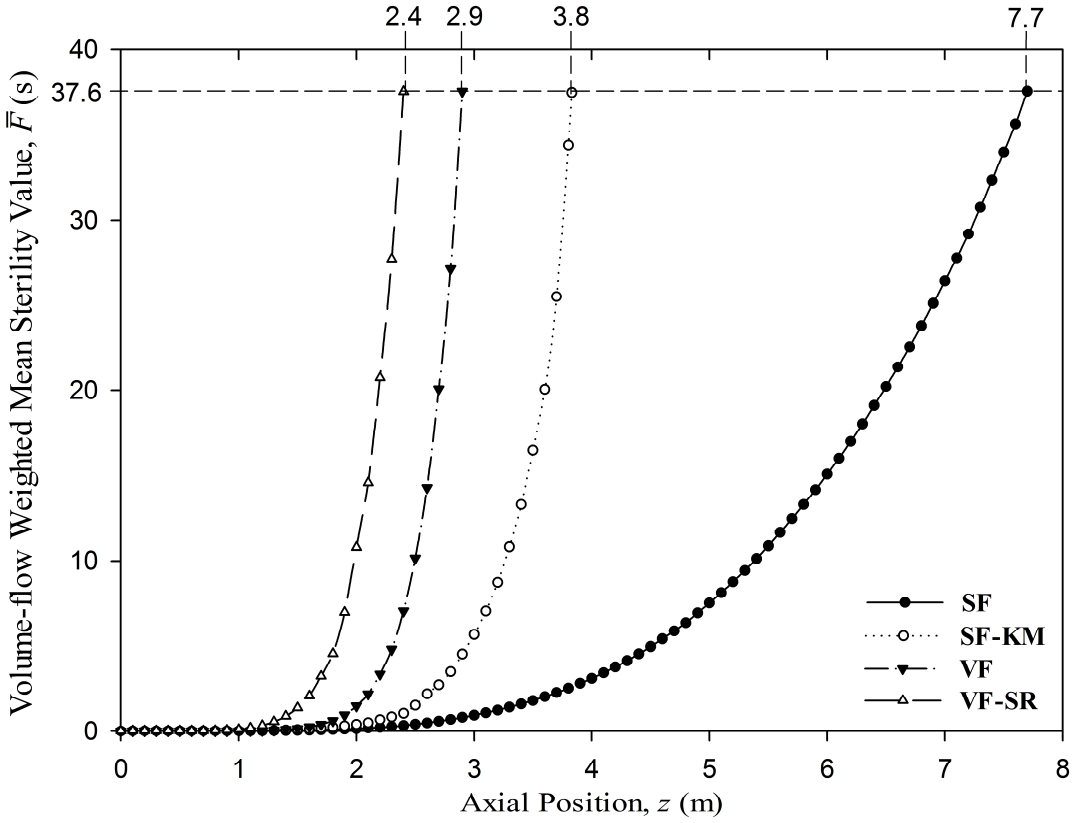

Figure 12. Axial profile of mean F-value in heating tubes with different flow regimes achieving the same mean sterility ($\bar{F}$ = 37.6 s) at the exit section.

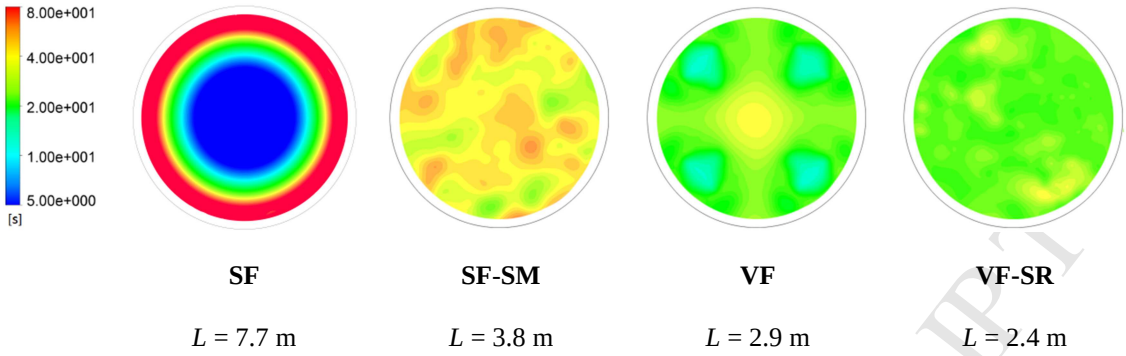

Figure 13. Radial contour plot of C-value at the exit section of heating tubes with different flow regimes achieving the same mean sterility ($\bar{F}$ = 37.6 s) at the exit section (note that the red colour in the **SF** plot is ~ 4-fold greater than the top end of the scale).

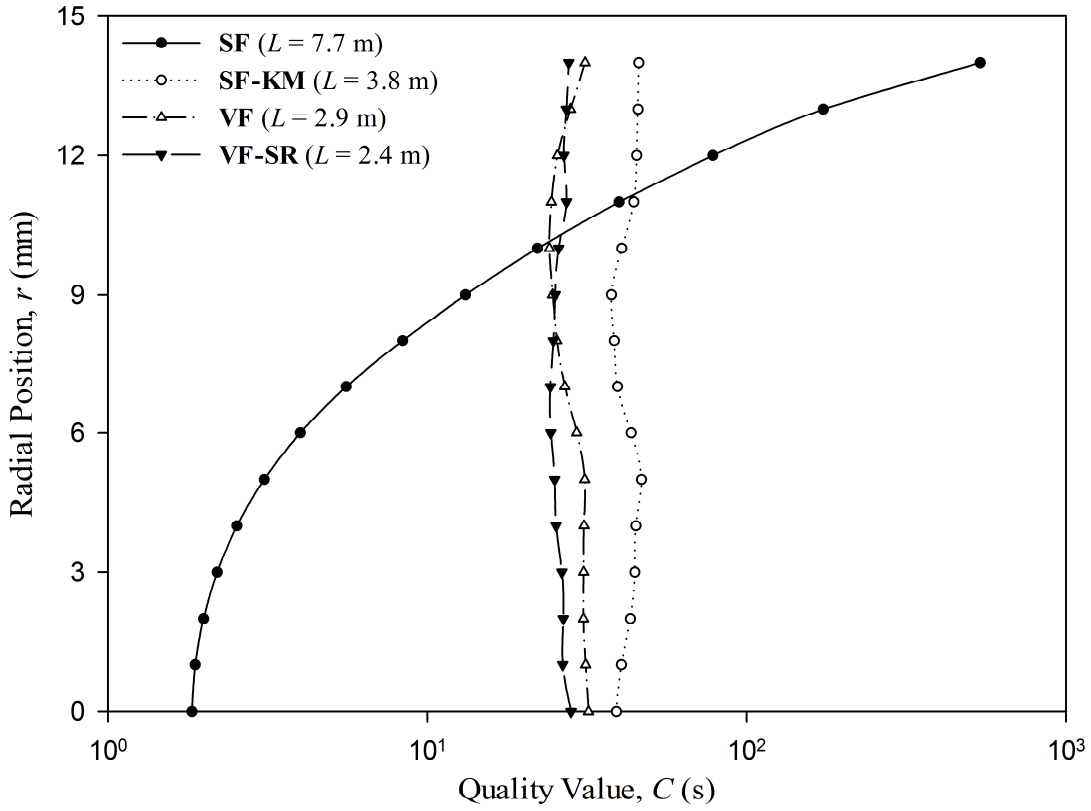

Figure 14. Radial profile of azimuthally-averaged C-value at the exit section of heating tubes with different flow regimes achieving the same mean sterility ($\bar{F}$ = 37.6 s) at the exit section.

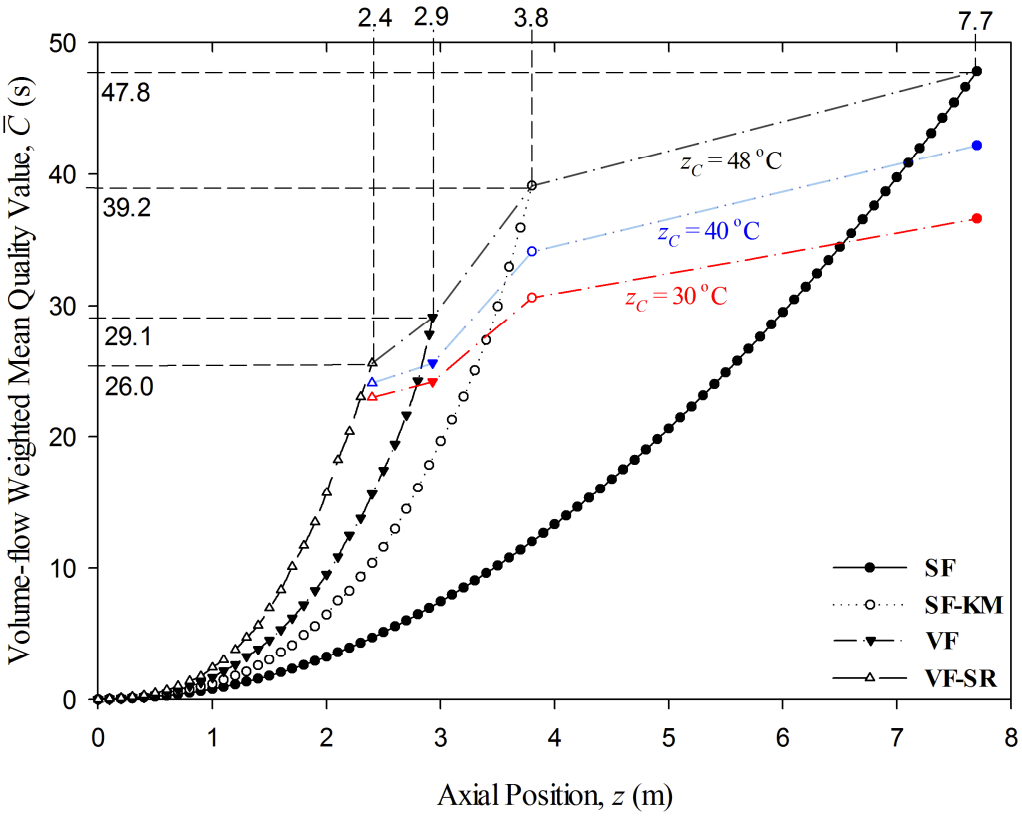

Figure 15. Axial profile of mean C-value in heating tubes with different flow regimes achieving the same mean sterility ($\bar{F}$ = 37.6 s) at the exit section.

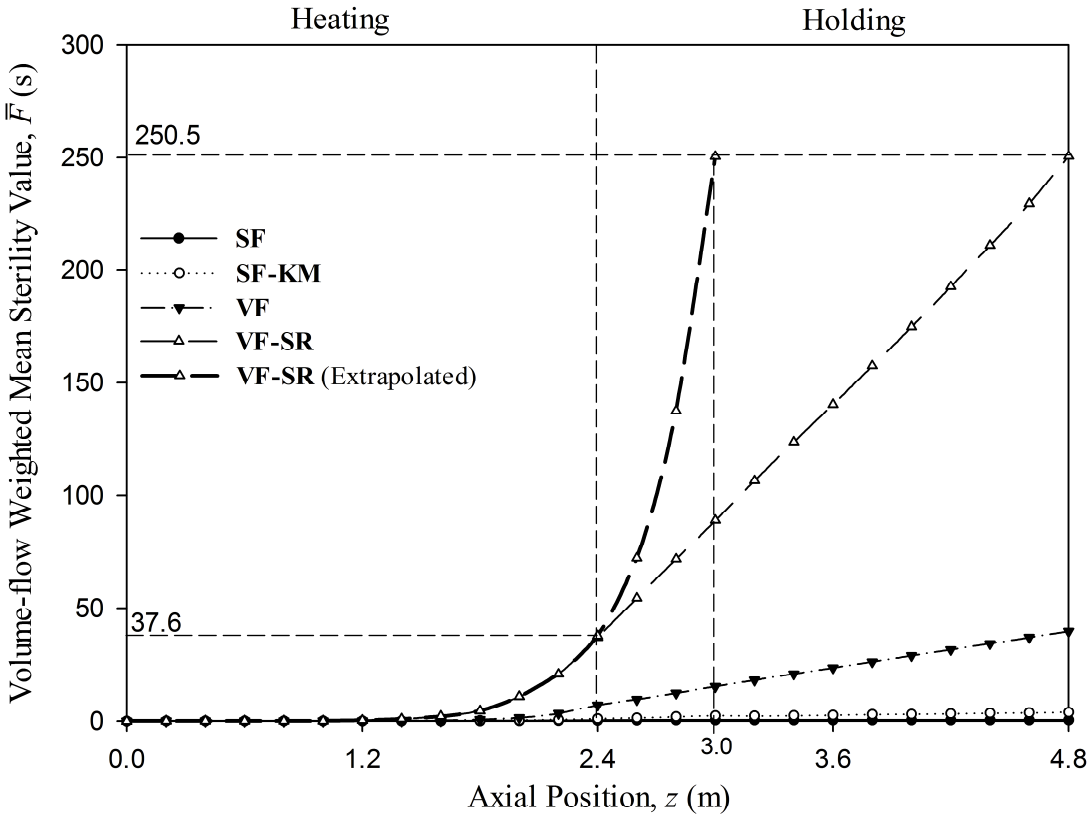

Figure 16. Development of mean F-value along heating and holding tubes.

Table 1. Process parameters used in simulations.

L (mm)	D (m)	T_{in} (°C)	T_w (°C)	$\bar{w}$ (m s^{-1})	k_0 (Pa s)	E_a (J mol^{-1})	R_g (J mol^{-1} K^{-1})	ρ (kg m^{-3})	C_p (J kg^{-1} K^{-1})	λ (W m^{-1} K^{-1})	$\mu = k_0 \exp\left(\frac{E_a}{R_g T}\right)$ (Pa s)	
											20°C	140°C
2400	0.03	20	140	0.04	5.0×10^{-7}	35000	8.314	998	4180	0.668	0.868	0.0134

Table 2. Dimensions of Kenics static mixer (Figure 1(*d*)).

Segment length (mm)	Gap width (mm)	Element length (mm)	Mixer diameter (mm)	Element thickness (mm)	Twist angle (rad)
50	2.5	45	30	1	π

Table 3. Process parameters used for CFD validation (Jung & Fryer, 1999).

Flowrate (m^3 h^{-1})	Density (kg m^{-3})	Viscosity (Pa s)	Specific heat (J kg^{-1} K^{-1})	Thermal conductivity (W m^{-1} K^{-1})	Inlet temperature (°C)	Heating temperature (°C)	Heating length (m)
0.1	998	0.001	4180	0.6	60	140	12

Table 4. Mean sterility and quality in the heating tube (L = 2400 mm).

	SF	**SF-KM**	**VF**	**VF-SR**
$\bar{F}$ (s)	0.32	1.2	7.2	37.6
$C_{v\text{-}F}$ (-)	3.75	1.58	1.33	1.09
$\bar{C}$ (s)	4.7	10.8	15.0	26.0
$C_{v\text{-}C}$ (-)	1.69	0.28	0.27	0.14

Table 5. Mean quality corresponding to the same mean sterility at exit ($\bar{F}$ = 37.6 s).

	SF	**SF-KM**	**VF**	**VF-SR**
$\bar{C}$ (s)	47.8	39.2	29.1	26.0
$C_{v\text{-}C}$ (-)	1.45	0.27	0.23	0.14
L (m)	7.7	3.8	2.9	2.4

Highlights

- Transverse vibration induces strong chaotic advection in viscous flow
- Chaotic advection enhances wall heat transfer and radial temperature uniformity
- Chaotic advection enables high levels of sterility to be achieved in short heating tubes
- Chaotic advection leads to quasi-uniform sterility with minimum loss of quality
- Thermal processing with chaotic advection flow may obviate the need for a holding stage